Evaporation and Combustion of Suspended Droplets with Buoyancy-Driven Flows

E. Cipriano*, A. Frassoldati*, T. Faravelli, A. Cuoci
edoardo.cipriano@polimi.it
*CRECK Modeling Lab, Department of Chemistry, Materials, and Chemical Engineering "G. Natta", Politecnico di Milano, Piazza Leonardo da Vinci, 32, Milano, 20133, Italy

Abstract
Numerical models for droplet combustion typically assume spherical symmetry, simplifying the fluid dynamics in favor of a detailed description of the combustion chemistry. This study relaxes that hypothesis by presenting a comprehensive numerical framework that includes: i) interface-resolved evaporation; ii) surface tension effects; iii) complex gas-phase kinetics; iv) radiation. This model employs the volume-of-fluid approach for the description of the two-phase system, and it enables the description of deformable droplets, in motion or suspended on a solid fiber. Despite the increased computational time, this model can directly resolve multidimensional phenomena, such as buoyancy-driven flows, droplet deformation, liquid internal recirculation, and non-spherical flames. This research helps to improve our understanding of droplet combustion dynamics, and it can be used to correct predictions from simplified models, accounting for multidimensional fluid dynamics phenomena.

Introduction
Alternative liquid fuels are recently studied as possible alternatives to fossil fuels. To deepen our understanding of the combustion of alternative liquid fuels we must combine the experimental investigation with mathematical models able to predict the correct consumption dynamics of fuel droplets. This work proposes a comprehensive numerical model that can simulate phase change in a gas-liquid system, assuming low Mach number, constant ambient pressure, subcritical conditions, and variable thermodynamic and transport properties. The resulting model is used to simulate isolated droplets suspended on a solid fiber at different gravity conditions. This configuration, widely used in experimental works, helps to simplify the spray combustion problem by neglecting the interactions between different droplets, and by focusing on the evaporation and combustion characteristics of a single droplet. The big novelty with respect to the previous literature works is that, in this study, we pursue the direct solution of the multidimensional system without relying on sub-grid-scale correlations.

Governing Equations
The control volume over which the system of equations is solved comprises two immiscible phases separated by a zero-thickness interface. The characteristic

function H is used to distinguish between the two phases:

$$H(\boldsymbol{x},t)=\begin{cases}1 & \text{if liquid phase}\\ 0 & \text{if gas phase}\end{cases} \tag{1}$$

where $\boldsymbol{x}$ is the space coordinate, while t is the generic simulation time.
The transport of the gas-liquid interface obeys the equation [1]:

$$\frac{DH}{Dt}=\frac{\partial H}{\partial t}+\boldsymbol{u}_{\boldsymbol{\Gamma}}\cdot\nabla H=0 \tag{2}$$

where $\boldsymbol{u}_{\boldsymbol{\Gamma}}$ is the interfacial velocity. The governing equations for each phase derive from a set of conservation laws on mass, momentum, chemical species, and mass fractions [2]:

$$\nabla\cdot\boldsymbol{u}=\beta\frac{DT}{Dt}+M\sum_{i=1}^{NS}\frac{1}{M_i}\frac{D\omega_i}{Dt} \tag{3}$$

$$\rho\frac{D\boldsymbol{u}}{Dt}=-\nabla\cdot\boldsymbol{\tau}-\nabla p_d-\boldsymbol{g}\cdot\boldsymbol{x}\nabla\rho \tag{4}$$

$$\rho\frac{D\omega}{Dt}=-\nabla\cdot\boldsymbol{j_i}+r_iM_i \tag{5}$$

$$\rho Cp\frac{DT}{Dt}=-\nabla\cdot\boldsymbol{q}-\left(\sum_{i=1}^{NS}Cp_i\boldsymbol{j_i}\right)\cdot\nabla T+\dot{Q}_r+\nabla\cdot\dot{\boldsymbol{q}}_{rad} \tag{6}$$

which are solved for the velocity $\boldsymbol{u}$, pressure p, temperature T, and chemical species mass fractions ω_i, while the density ρ is updated using an Equation of State. According to the low-Mach formulation, the pressure gradients in the continuity equation are neglected with respect to the expansion due to temperature and composition changes. The term β is the thermal expansion coefficient, while M and M_i are the molecular weight of the mixture and of the chemical species i, respectively. The viscous stress tensor in the momentum equation is computed by neglecting the compressible part: $\boldsymbol{\tau}=-\mu(\nabla u+(\nabla u)^T)$ where μ is the dynamic viscosity. The pressure is linked to the dynamic pressure p_d by the hydrostatic contribution: $p_d=p-\rho\boldsymbol{g}\cdot\boldsymbol{x}$, with $\boldsymbol{g}$ the gravitational acceleration. Eq. (5) comprises the diffusive fluxes, computed using Fick's law, and the reaction rate r_i. The temperature equation (6) includes the heat conduction term $\boldsymbol{q}$, calculated using Fourier's law, the enthalpy changes due to the chemical species diffusion, where Cp is the heat capacity, the heat of reaction $\dot{Q}_r$ and the radiation heat fluxes $\dot{q}_{rad}$. In this work we neglect the heat transfer between the solid suspender and the gas-liquid system. Therefore, the only effect of the solid fiber that we consider is the droplet suspension by the action of the surface tension force.

Equations (3-6) are valid in the gas and in the liquid phase separately, but they must

be coupled with appropriate gas-liquid interface boundary conditions, obtained by integrating Eq. (3-6) across a portion of the interface. Introducing the jump notation for a generic variable: $[\phi] = \phi_l - \phi_g$ the following set of jump conditions is obtained [3]:

$$[\boldsymbol{u}]_\Gamma \cdot \boldsymbol{n}_\Gamma = \dot{m}[1/\rho]_\Gamma \tag{7}$$

$$[p]_\Gamma = \sigma\kappa - \dot{m}[\boldsymbol{u}]_\Gamma \cdot \boldsymbol{n}_\Gamma + [\boldsymbol{\tau} \cdot \boldsymbol{n}_\Gamma]_\Gamma \cdot \boldsymbol{n}_\Gamma \tag{8}$$

$$[\rho(\boldsymbol{u} - \boldsymbol{u}_\Gamma) \cdot \boldsymbol{n}_\Gamma]_\Gamma = 0 \tag{9}$$

$$[\rho\omega_i(\boldsymbol{u} - \boldsymbol{u}_\Gamma) \cdot \boldsymbol{n}_\Gamma + \boldsymbol{j}_i \cdot \boldsymbol{n}_\Gamma]_\Gamma = 0 \tag{10}$$

$$[\lambda\nabla T \cdot \boldsymbol{n}_\Gamma]_\Gamma = \sum_{i=1}^{NS} \dot{m}\Delta h_{ev,i} + \epsilon\sigma_{SB}(T_\infty^4 - T_\Gamma^4) \tag{11}$$

which is solved to obtain every information about the interface: vaporization rate $\dot{m}$ for each chemical species, interface temperature, mass fractions, and mole fractions. The velocity jump is due to the Stefan flow contribution, the pressure jump includes the surface tension force, where σ is the surface tension coefficient, while κ is the interface curvature. The terms n_Γ and t_Γ indicate the interface normal and tangential vectors, respectively. The interface enthalpy balance (Equation 11) includes the interface radiation term, where ϵ is the emissivity, σ_{SB} is the Stefan-Boltzmann constant, while T_∞ is the gas phase bulk temperature.
The interface is assumed to be at thermodynamic equilibrium conditions, and therefore, the system of jump conditions is closed by including the vapor-liquid equilibrium relationships, which expresses the continuity of the chemical species fugacity f_i and of the temperature across the interface.

$$[f_i]_\Gamma = 0 \tag{13}$$

$$[T]_\Gamma = 0 \tag{14}$$

In this work, Raoult's law is used for the VLE, assuming an ideal liquid mixture, an ideal gas mixture, and negligible Poynting correction.

Numerical Discretization

The set of equations described in the previous section is integrated using the Finite Volume Method on adaptive Cartesian grids, using quad/octree discretization [4]. The transport of the interface is performed using the geometric Volume-of-Fluid approach [3], which discretizes Eq. (2) by keeping the sharp nature of the characteristic function taking advantage of the planar interface reconstruction. The jump conditions (7-11) are introduced into the governing equations (3-6) using the Whole Domain Formulation [3], by expressing them as source terms localized at the gas-liquid interface. Details about the numerical methods for solving the

incompressible multicomponent phase change equations are reported in Cipriano et al. [5], whose model is extended in this work by including variable thermodynamic and transport properties, low-Mach compressibility effects, and chemical reactions.

Results: Droplet Evaporation

The model presented in this work was validated with pure evaporation cases by comparing our simulation results with experimental data and with a well-validated 1D model that assumes spherical symmetry [6].

The first test case is the evaporation of a n-heptane droplet in microgravity at different pressure (1, 5, 10, 20 atm) and temperature (~450, 550, 650, 750 K) conditions. The initial droplet diameter is 0.7 mm, and the simulation is performed by exploiting the axial symmetry. Fig. 1 shows the trend of the square droplet diameter in time. We notice that our model and the 1D model are in excellent agreement at every operative condition. However, there is a delay between the numerical results and the experimental data which increases with pressure, and which is more evident for lower temperature conditions.

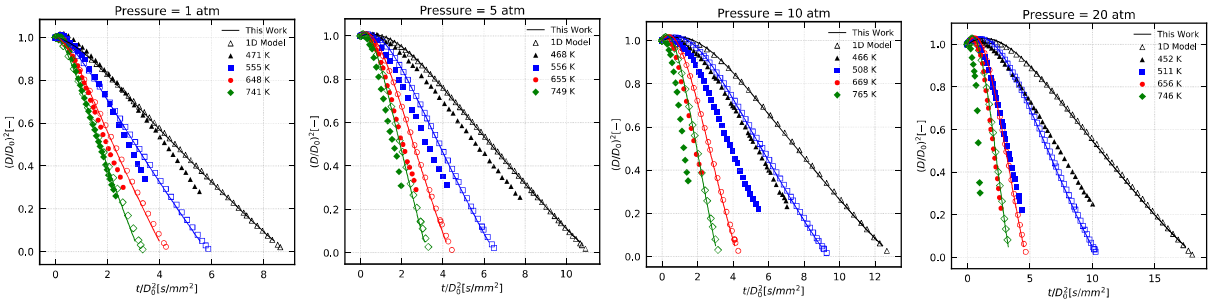

Figure 1: Square diameter decay in time for n-heptane droplet evaporation in microgravity.

The ability of our model to resolve droplets at different gravity conditions is exploited to explain the discrepancies between the numerical models and the experiments. To this purpose, we re-simulate the Nomura et. al [7] droplets at different gravity values: $1/100\boldsymbol{g}$, $1/10\boldsymbol{g}$, $1\boldsymbol{g}$, where $\boldsymbol{g}$ is the Earth's normal gravity value, where the value of $1/100\boldsymbol{g}$ is the residual gravity measured by [7] for the parabolic flight experiments. Fig. 2 shows that the introduction of gravity shifts the numerical results toward the experimental data, with more intensity at high pressure and low temperature, in agreement with the functional dependency of the Grashof number, which measures the importance of the natural convective fluxes.

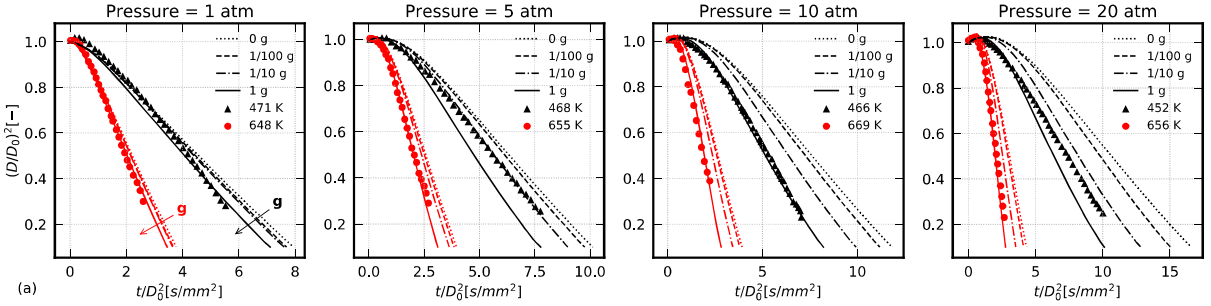

Figure 2: Effect of the residual gravity on the evaporation of n-heptane droplets.

The effects of the interface radiation and of the heat conduction from the solid fiber on Nomura et al. [7] droplets have already been studied by other authors. However, those studies cannot explain the pressure dependency of the gap between the experimental data and the numerical results, which was highlighted for the first time in this work using direct numerical simulations.
The evaporation of droplets in normal gravity conditions was validated by comparing our model with experimental data [8]. This test case considers n-decane droplets with different initial diameters (0.4, 0.52, 0.6, 0.7 mm), at ambient temperature 773 K, droplet initial temperature 328 K, at pressures 1 and 5 atm. Fig. 3 shows that our model captures the same trends of the experimental data for the droplet consumption rate at different initial diameters.

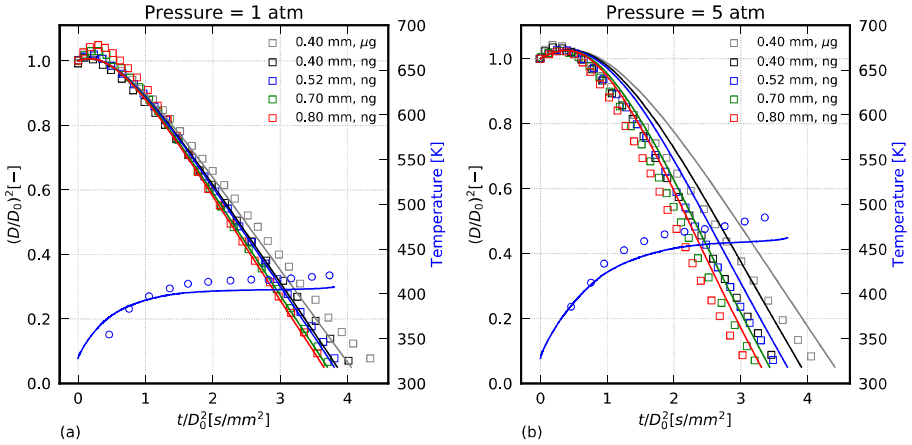

Figure 3: Square diameter decay in time for n-decane droplet evaporation in normal gravity.

Results: Droplet Combustion

The same study on the influence of pressure and buoyancy on the droplet consumption rate should be performed with combustion cases. Such study can highlight the different burning rates of droplets in microgravity and in normal gravity conditions, at different ambient temperatures and pressures. The results from this study are useful to obtain expressions and correlations that correct 0D and 1D models that cannot directly solve multidimensional phenomena. In this test case, we considered the combustion of methanol droplets at different pressures (5, 10, 15 atm), with an initial diameter of 0.5 mm. Fig. 4 reports the square droplet diameter in time from our model, both in microgravity and in normal gravity conditions. The comparison with OpenSMOKE++ shows a displacement that require further investigation, but both models show the same physical trend: in microgravity the burning rates of the droplets increases with increasing ambient pressure. In normal gravity conditions this effect is magnified, and the consumption of the droplets is strongly increased because of natural convective fluxes and because of the different flame position and geometry.

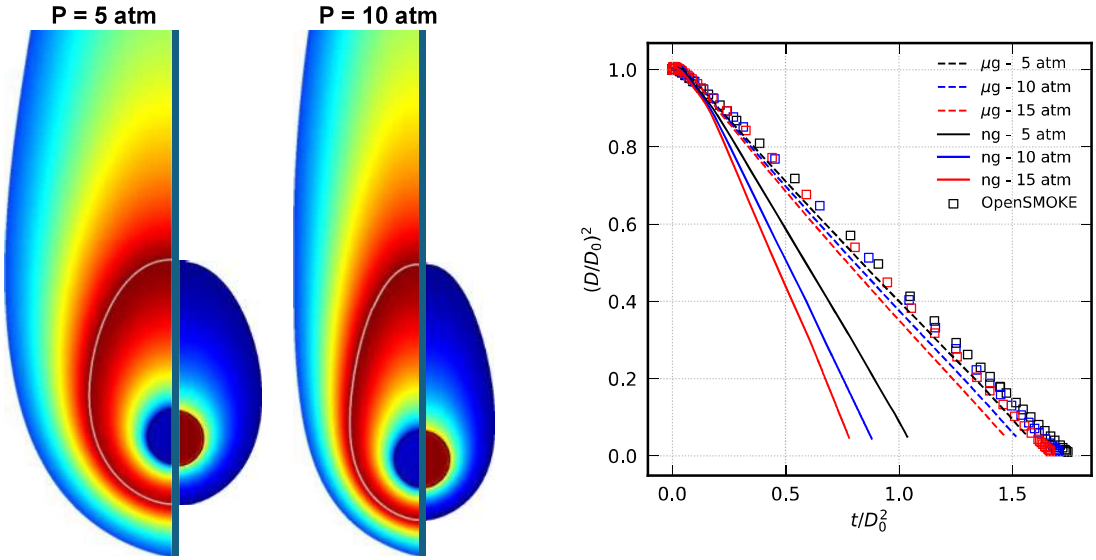

Figure 4: Maps of the temperature and fuel mass fraction (left); square diameter decay for the methanol combustion in microgravity and in normal gravity conditions (right).

References

[1] Drew, D.A., "Mathematical modeling of two-phase flow", *Annual review of fluid mechanics* 15: 261-291 (1983)

[2] Pember, R. B., Howell, L. H., Bell, J. B., Colella, P., Crutchfield, W. Y., Fiveland, W. A., & Jessee, J. P., "An adaptive projection method for unsteady, low-Mach number combustion", *Combustion Science and Technology* 140: 123-168 (1998)

[3] Scardovelli, R., & Zaleski, S., "Direct numerical simulation of free-surface and interfacial flow", *Annual review of fluid mechanics* 31: 567-603 (1999)

[4] Popinet, S., "Gerris: a tree-based adaptive solver for the incompressible Euler equations in complex geometries", *Journal of computational physics* 190: 572-600 (2003)

[5] Cipriano, E., Frassoldati, A., Faravelli, T., Popinet, S., & Cuoci, A., "Multicomponent droplet evaporation in a geometric volume-of-fluid framework", *Journal of computational physics* 507 (2024)

[6] Cuoci, A., Mehl, M., Buzzi-Ferraris, G., Faravelli, T., Manca, D., & Ranzi, E., "Autoignition and burning rates of fuel droplets under microgravity", *Combustion and Flame* 143:211-226 (2005)

[7] Nomura, H., Ujiie, Y., Rath, H. J., Sato, J. I., & Kono, M., "Experimental study on high-pressure droplet evaporation using microgravity conditions", *Proc. Comb. Inst.* 26:1267-1273 (1996).

[8] Murakami, Y., Nomura, H., & Suganuma, Y., "Experimental study on unsteadiness of n-decane single droplet evaporation and effect of natural convection on droplet evaporation at high pressures and temperatures", *Transactions of the japan society for aeronautical and space sciences, aerospace technology japan,* 19:647-653 (1996).